

Chemical-mechanical polishing performance of core-shell structured polystyrene@ceria/nanodiamond ternary abrasives on sapphire wafer

Chen Zhou^a, Xiangyang Xu^{a,b,*}, Lei Dai^a, Haiming Gong^a, Shuntian Lin^a

^a School of Minerals Processing and Bioengineering, Central South University, Changsha 410083, Hunan, PR China

^b Hunan Key Laboratory of Mineral Materials and Application, Changsha 410083, Hunan, PR China



ARTICLE INFO

Keywords:

Composite abrasive
Powders: chemical preparation
Sapphire substrates
Chemical mechanical polishing

ABSTRACT

Driven by electrostatic attraction, Ce⁴⁺ ions or/and positively charged detonation nanodiamond (DND) particles can absorb onto negatively charged polystyrene (PS) spherical colloids. Three types of core-shell structured composite abrasives, PS@CeO₂, PS@DND and PS@CeO₂/DND, can thus be assembled. When PS@CeO₂ and PS@DND were used to polish sapphire wafer at pad rotating speed of 120–150 r/min and load pressure of ~3 kg, the material removing rate (MRR) exceeded 1.0 µm h⁻¹, 10–20 % higher than unitary abrasives. The surface profile roughness (Ra) for wafer polished by these two composite abrasives was respectively 1.25 and 0.63 nm, which is superior to CeO₂ (Ra = 1.38 nm) and DND (Ra = 1.29 nm). When using PS@CeO₂/DND, the polishing interface area can be increased owing to the combined effect of elastic PS spheres and intensively coated CeO₂ and DND. Meanwhile, the synergistic mechanism of sapphire-CeO₂ chemical reaction and the strong mechanical abrasion of DND particles benefit the polishing efficiency. MRR for this ternary composite abrasive attained 1.4–1.7 µm h⁻¹ while sapphire can be smoothed to a sub-nanoscale roughness.

1. Introduction

Single crystal sapphire (α -Al₂O₃) substrate has excellent optical and mechanical properties such as electrical and dielectric properties, hardness and chemical corrosion resistance. It also possesses high transmittance of infrared rays, good wear resistance and excellent high-temperature stability [1–4]. Therefore, it has been increasingly applied in high-tech fields such as solid lasers, infrared windows, semiconductor chips, missile domes and transparent armours [5–8]. However, owing to its high hardness (9 on the Mohs scale), brittleness and chemical rigidity, it is a challenge to obtain sapphire wafer with qualified surface roughness (Ra) [9,10]. As the most widely used planarization approach, chemical mechanical polishing (CMP) has been proved to be an option for sapphire polishing as it can effectively control the global and local flatness of the machining surface [11–13].

The performance of varied abrasives such as colloidal silica [14–16], nanodiamond [17,18], ceria [19] and alumina [20,21] in sapphire surface planarization has been studied. Owing to its good dispersion, narrow size distribution and low-cost, colloidal silica has been widely used in CMP process [22], despite its comparatively lower material removal rate (MRR) and less satisfying surface quality [13,23]. To

achieve better performance than corrosive CMP with NaOH as a pH regulator, Zhang et al. [24] proposed a novel green CMP by mixing silica nanoparticles with triethanolamine, sodium metasilicate nonahydrate and deionized water. The Ra of sapphire was reduced to 0.11 nm while the MRR attained 3.31 µm/h. Their group developed as well a variety of silica slurries containing different environment friendly ingredients to polish copper [25], nickel alloys [26], CdZnTe crystals [27] and even the single crystal diamond [28], which upgraded the performance of silica-based CMP and proposed a solution for clean polishing. In the attempt to process glass-ceramics, high MRR can be achieved with detonation nanodiamond (DND) possessing high mechanical abrasive capacity [17]. Yet, workpieces were usually seriously scratched by hard abrasives, such as DND and alumina abrasives, reaggregated amidst the polishing processes [20,29]. In the practice of hard abrasives, the additives and the process regulation are usually critical to actualize ultra-smooth surface and damage-free machining [30]. CeO₂ abrasive possesses many advantages, such as high polishing efficiency, excellent polishing quality and long service life. However, its size distribution is always somewhat broad and the clusters are of irregular shape [31], which may result in serious scratches. Therefore, to synthesize nano-scaled ceria abrasives with uniform particle size distribution and even

* Corresponding author. School of Minerals Processing and Bioengineering, Central South University, Changsha 410083, Hunan, PR China.

E-mail address: xuxiangyang@csu.edu.cn (X. Xu).

morphology is constantly a challenge.

Core/shell-structured organic@inorganic composite abrasives (OICAs) [32,33] have been introduced into CMP processes in recent years [34,35]. The influence of abrasive factors, including OICAs' shape and size, shell thickness and morphology, has been investigated [34]. Chen et al. [36] prepared PS/CeO₂ abrasives with different shell thickness and studied their performances in polishing SiO₂ films. The results showed that compared with those processed by free CeO₂ abrasives, PS/CeO₂ polished films possesses improved surface quality. Their studies [37,38] also show that, the organic core benefit the reduction of both Ra and mechanical damage, while the inorganic CeO₂ or mesoporous silica shells are conducive to improve MRR. By hydrolyzing tetraethoxysilane (TEOS), silica can condensate on positively charged PS colloids and obtain PS@SiO₂ abrasives. When used to polish copper substrate, the root mean square (RMS) roughness was decreased from 4.27 nm to 0.56 nm, while the MRR was as well higher than that of SiO₂ abrasives [32].

In this study, we synthesized PS@CeO₂, PS@DND and PS@CeO₂/DND, composite abrasives of core-shell structure, and investigated their polishing performance. Adopting a soap-free emulsion polymerization approach, negatively charged PS colloidal microspheres were prepared. Then, by introducing cerium precursor, cerium ions can precipitate on PS granules and eventually construct PS@CeO₂ core-shell particles. The as-received DND powder were finely ground and modified to obtain suspensions containing well-dispersed and positively charged DND particles. Driven by electrostatic interaction between PS and DND, PS@DND core-shell abrasives were assembled. The ternary composite abrasive, PS@CeO₂/DND, can be fabricated by depositing deagglomerated DND particles onto pre-synthesized PS@CeO₂. According to MRR and Ra values, when used to polish sapphire wafer, these composite abrasives, especially, PS@CeO₂/DND, show better polishing performance than the unitary abrasives.

2. Material and methods

2.1. Chemicals and materials

Styrene monomer (C₈H₈, ≥99 %) was purchased from Shanghai Aladdin Bio-Chem Technology Co., Ltd. (Shanghai, China). Cerium nitrate (Ce(NO₃)₃·6H₂O, ≥99 %), citric acid (C₆H₈O₇·H₂O, ≥99 %), sodium hydroxide (NaOH), hydrochloric acid (HCl, 37 %), hexamethylenetetramine (HMT, C₆H₁₂N₄, ≥99%) and hexadecyltrimethylammonium bromide (CTAB, C₁₆H₃₃(CH₃)₃NBr, ≥99 %), were purchased from Sinopharm Chemical Reagent Co., Ltd. (Beijing, China). K₂S₂O₈ (KPS, ≥99 %) and anhydrous ethanol (C₂H₅OH, ≥99 %) were bought respectively from Tianjin Kemiou Chemical Reagent Co., Ltd. (Tianjin, China) and Tianjin Hengxing Chemical Reagent Co., Ltd. (Tianjin, China). The sapphire wafers (1-inch standard raw wafers) were provided by Sichuan Xintong New Material Co., Ltd. (Wenchuan, China). The pristine DND powder (diamond phase ≥ 95 %) was provided by Chengdu Fortune Myriad Diamond Nano-Tech Co., Ltd. (Chengdu, China). The digital image of as-received DND powder is shown in Electronic Supplementary Information (ESI) Fig. S1(a).

2.2. Synthesis of PS microspheres and composite abrasives

The as-received styrene monomer was washed using 10 wt% NaOH solution to remove phenolic inhibitor, then, the alkaline styrene solution was washed for multiple times with deionized water until reaching a neutral level. Then, 10 mL de-inhibited styrene monomer and 200 mL deionized water were added into a 250 mL three-necked flask with round bottom, and ventilated with N₂ for 20 min to drive off oxygen. Thereafter the flask was heated in water bath at 80 °C. After 0.2 g KPS was added, N₂ was ventilated sustainedly for another 21 h till reaching reflux stabilization. PS emulsion was thus prepared after this polymerization process.

These composite abrasives were synthesized using PS suspension, modified small DND clusters and cerium salt as the main reactants. Scheme 1 illustrates the fabrication processes of core-shell structured abrasives.

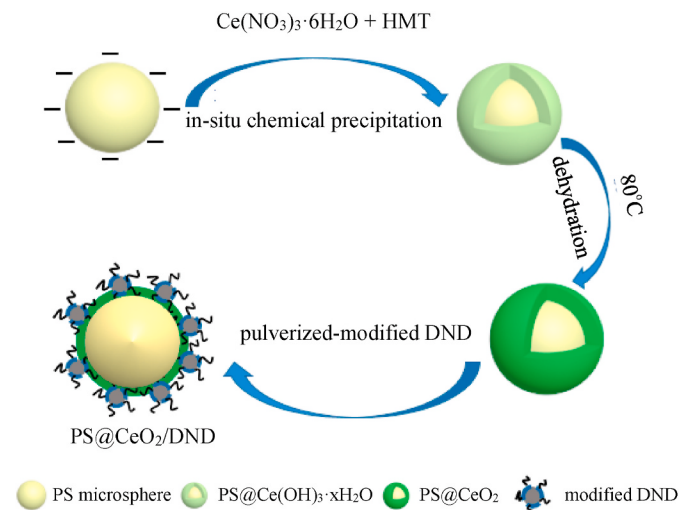
PS suspension (4 mL) at the concentration of 30 g L⁻¹ was added into a glass beaker containing 200 mL deionized water, and the mixture was sonicated for 10 min to disperse PS colloids. Then, a certain amount of Ce(NO₃)₃·6H₂O was added into the solution by keeping the Ce (NO₃)₃·6H₂O/HMT molar ratio as 1:5. The mixture was heated at 80 °C and stirred for 2.5 h. Then, before dried at 100 °C for 4 h, the resultant precipitates were centrifuged and washed by deionized water and anhydrous alcohol for 3 times. PS@CeO₂ abrasives with varied CeO₂ content were synthesized with 0.0023, 0.0058, 0.0115, 0.0173 and 0.0345 mol L⁻¹ Ce(NO₃)₃·6H₂O, among which the sample prepared using 0.0115 mol L⁻¹ Ce(NO₃)₃·6H₂O is used to discuss the properties of composite abrasives.

A homogeneous suspension of deagglomerated DND clusters was prepared, and the digital images of suspensions for pristine DND and deagglomerated DND are shown in ESI Fig. S1(b). The processing procedure was described in ESI Fig. S1c. Mixed with CTAB (2 × 10⁻³ mol L⁻¹) and stirred for 1 h, the ground particles were modified. PS@DND composite particle was prepared following the similar procedure for PS@CeO₂. NaOH solution (0.1 mol L⁻¹) was added into the 200 mL pre-conditioned PS solution to adjust the pulp pH as 10–11, then a certain volume of DND suspension (5 g L⁻¹) was added. Then the mixture was heated in water bath at 80 °C and stirred for 2.5 h. PS@DND prepared with 0.75 g L⁻¹ DND was chosen to discuss abrasive properties.

Similarly, 0.0115 mol L⁻¹ of Ce(NO₃)₃·6H₂O was added in the 200 mL pre-conditioned PS solution, keeping the molar concentration ratio of Ce(NO₃)₃·6H₂O and HMT being 1:5. The solution was heated at 80 °C and stirred for 2.5 h. Then, NaOH solution (0.1 mol L⁻¹) was added in the PS@CeO₂ homogeneous suspension to adjust pH value to 10–11. After that, 30 mL CTAB-modified DND suspension (5 g L⁻¹) was added into the PS@CeO₂ homogeneous suspension, and the mixed solution was then stirred for another 2.5 h at 80 °C, with which PS@CeO₂/DND abrasives were prepared.

2.3. Characterization on raw materials and abrasives

Field-emission scanning electron microscopy (FESEM) was employed to visualize the morphology of DND crystallites, PS microspheres, composite particles and sapphire substrates. TESCAN MIRA3 (TESCAN, Brno, Czech) equipped with an Oxford X-Max20 energy system at an



Scheme 1. Schematic illustration for synthesis procedure of composite abrasives.

accelerating voltage of 20 kV was used.

Transmission electron microscopy (TEM) was adopted to study the morphology of PS colloids and the core-shell structured composite particles. Tecna G20ST (FEI, Hillsboro, USA) microscope with LaB₆ filament was adopted. The powder samples were dispersed in ethanol and dripped onto the carbon film supported by copper grid. High-resolution TEM (HRTEM) digital images were shot by a CCD camera and the DigitalMicrograph® software from Gatan was used to measure the lattice parameters.

Particle size distributions of PS microspheres, DND samples and composite abrasives dispersed in aqueous suspensions was measured using Zetasizer Nano ZS (Malvern Instruments Ltd., Malvern, UK), with which the ζ potential of particles dispersed in aqueous solutions was as well analyzed. The ζ -pH curves were obtained over the pH range of 1.0–12.0. The pH value was regulated using deionized water and HCl (0.1 mol L⁻¹) or NaOH (0.1 mol L⁻¹) aqueous solutions.

X-ray diffraction (XRD) analyses were conducted to characterize the structure of pristine and composited materials by using DX-2700 (Dandong Haoyuan Instrument Co. Ltd., Dandong, China). Under the operation voltage and current as 40 kV and 40 mA, respectively, Cu K α ($\lambda = 1.54178 \text{ \AA}$) was used as the radiation source. All samples were measured over the 2θ angle ranging from 3° to 80° at 4°/min.

Thermogravimetric (TG) analysis and differential thermal analysis (DTA) were conducted under air atmosphere from 30 to 800 °C at a heating rate of 10 °C min⁻¹ using a DSC Q2000 thermal analyzer (TA instruments, New Castle, USA).

Fourier transform infrared spectroscopy (FTIR) was used to characterize the surface functional groups. The spectra were recorded over the wavenumber range of 4000 to 400 cm⁻¹ on a Nexus 670 spectrometer (Nicolet Instrument Corporation, Madison, USA). The samples are blended with KBr powder and pressed to prepare pellets for sampling at room temperature.

Using Thermo Scientific K-Alpha⁺ (Thermo Fisher Scientific, Waltham, USA), X-ray photoelectron spectroscopy (XPS) spectra of the as-collected polishing residue. A monochromatized Al K α radiation (1486.6 eV) was used as the X-ray source. Besides the survey, narrow spectra of main elements were acquired with the energy step size of 0.1 eV.

2.4. CMP experiments

Polishing experiments were performed with ZDHP-30 B, a polishing machine manufactured by Nanjing Lisheng Instrument Co. Ltd. (Nanjing, China). A porous polyurethane polishing pad was used. The size for as-received sapphire wafers were φ25.4 mm × 0.45 mm, and the polishing parameters were set as shown in Table 1. After polishing, the wafers were rinsed with deionized water and dried in a dry oven.

The masses of sapphire wafers were measured by an analytical balance for three times to calculate the MRR according to the following formula (Eq. (1)):

$$\text{MRR} = \frac{10^7 \times \delta m}{\rho \pi R^2 t} \quad (1)$$

where Δm (g) is the mass change of sapphire wafer before and after polishing, R (cm) is the radius of sapphire wafer, t (min) is the polishing time, ρ is the density of sapphire wafer (3.98 g cm⁻³), and the unit for

Table 1
Sapphire CMP polishing parameters.

Parameter	Specifications
Polishing time	20 min
Polishing pressure	1–5 kg
Pad rotating speed	60–150 rpm
Slurry flow rate	50 mL min ⁻¹
Abrasives contents	1 wt%

MRR is nm min⁻¹. The influence of rotating speed and down force on polishing efficiency was investigated. For each single parameter, three parallel tests were conducted at the same conditions. The average MRR and the standard deviation were used to evaluate their influence. The polished surface topographical and roughness (Ra) were measured by atomic force microscopy (AFM, Multimode V, Veeco, Plainview, USA) with the contacting mode.

3. Results and discussion

3.1. Morphology and size distribution of PS microspheres and DND clusters

SEM images of PS, pristine DND and deagglomerated DND are shown in Fig. 1. Particle size distribution curves of these samples are superimposed on the images. As it can be seen from Fig. 1(a) and (b), distributed in a narrow size range of 350–420 nm, the as-produced PS microspheres are of well-dispersed homogeneous spherical morphology.

As is shown in Fig. 1(c), although there is a portion of small particles of 100–300 nm in granularity, the aggregation of primary DND is serious, while the average particle size of primary DND is as high as ~0.8 μm . To assemble DND onto PS microsphere, it is crucial to reduce its granularity and improve its dispersion performance. Fig. 1(d) shows that, after deagglomeration, DND particles distributed more homogeneously, and the average particle size was reduced to ~50 nm.

3.2. Surface potential of PS and DND

Fig. 2 shows the variation of ζ potential for PS microspheres, as-deagglomerated DND and CTAB-modified DND in aqueous solution with pH value ranging from 1.0 to 12.0. According to its ζ -pH curve, PS microspheres were negatively charged, as the ζ potential kept below -20 mV over the whole pH range. With the increase of pulp alkalinity, its ζ potential descended gradually and the dispersion became more stable. The ζ potential for PS microspheres was below -30 mV when pH value exceeds 9.

The ζ potential for as-deagglomerated DND is ~30 mV though the whole pH range, except descending continuously in the alkaline environment. After modified by CTAB, DND particles have even higher positive ζ potential (~40 mV). Especially, in alkali aqueous solution, the ζ potential of CTAB-modified DND can ascend to as high as ~50 mV at pH 11, indicating the adsorption of this cationic surfactant on DND, which guaranteed the stable dispersion of DND. With the increase of absolute values of ζ potential, the electrostatic attraction between positively charged DND and negatively charged PS was intensified, which can promote their self-assembly.

3.3. Structure and composition of composite abrasives

As shown in ESI Fig. S2, the as-prepared abrasives and their corresponding suspensions were varied in the color. The phase composition of these samples was investigated. Fig. 3(a) shows XRD patterns of PS microspheres and composite abrasives. There is a typical a diffuse peak at 2θ angle of ~20° on the PS pattern, which can be attributed to its amorphous crystal structure [36,39,40]. Five diffraction peaks observed at 2θ angle of 28.6°, 33.1°, 47.6°, 56.3° and 59.1° on PS@CeO₂ and PS@CeO₂/DND patterns, concur with those on the pattern of CeO₂ powder we prepared following the sol-gel process with cerium nitrate and citric acid as the reactants (ESI Fig. S3). Conforming to the powder diffraction file (PDF) card (JCPDS 34–0394) [41], they are typical diffraction peaks for (111), (200), (220), (311) and (222) facets of fcc-structured ceria. It proved that, following the chemical precipitation and drying processes, cubic fluorite-structured CeO₂ crystallites were adhered on PS, as the XRD characteristic peaks of CeO₂ are strong, while no peaks of heterogeneous components were observed.

Two diffraction peaks at 2θ angle of ~20.0° and ~42.3° can be

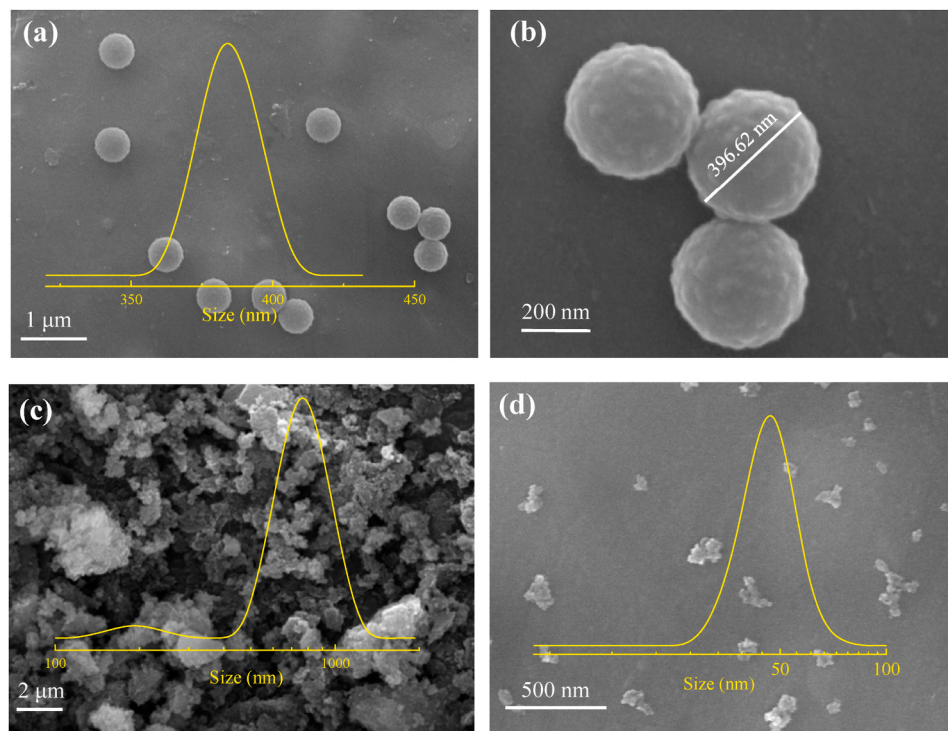


Fig. 1. FESEM images and particle size distribution (inset curves) of PS microspheres (a, b), primary DND (c) and deagglomerated DND particles (d).

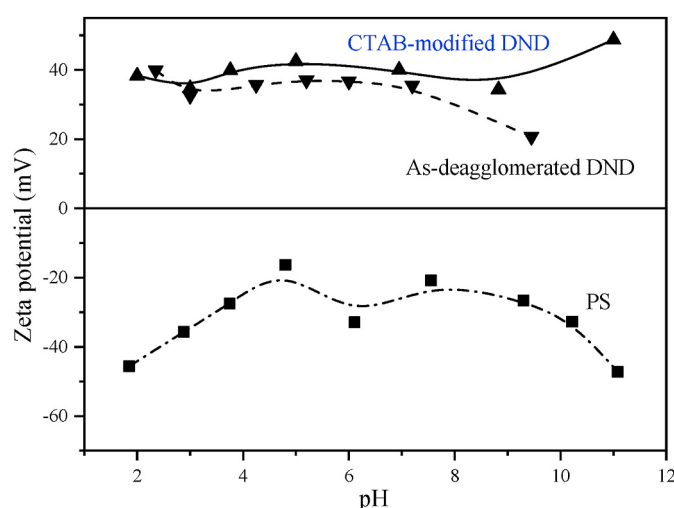


Fig. 2. Surface ζ potential of deagglomerated DND, CTAB-modified DND and PS at different pH value.

observed on the pattern of PS@DND. The former proved the existence of PS microspheres, while the latter is a characteristic diamond peak ((111) facet of fcc diamond structure) [17,18]. It verified the composition of PS@DND. On the pattern of PS@CeO₂/DND, typical ceria and diamond diffraction peaks were observed, testified that DND and CeO₂ has co-deposited on PS.

The quantity of reactants has remarkable influence on abrasive composition. XRD patterns of PS@CeO₂ with varied amount of cerium nitrate precursor and those of PS@DND by adding varied DND concentration were shown in ESI Figs. S4 and S5. The corresponding parameters for PS@CeO₂ and PS@DND preparation were listed in ESI Tables S1 and S2. When 0.0023 mol L⁻¹ Ce(NO₃)₃·6H₂O was added, both the broad PS peak ($2\theta = \sim 20^\circ$) and ceria peaks can be observed. With the increase of Ce⁴⁺ ions, the PS peak weakened stepwise. When Ce

(NO₃)₃·6H₂O attained 0.0115 mol L⁻¹, PS peak was no longer detectable. The vanish of PS peak occurred likewise on the patterns of PS@CeO₂/DND and composites prepared in some other studies [40,42]. The intensity of PS peaks for PS@DND declined as well along with the increase of DND content, while the diffraction for (111) (even (220)) facet emerged and intensified gradually. The weakening of PS peaks may be attributed to the stepwise coating of inorganic shells.

According to TG-DTA curves (Fig. 3(b)), there are two weight-loss stages (correspondingly, two endothermic peaks) for PS@CeO₂ and PS@DND. The first one, i.e., the first endothermic reaction, can be attributed to PS decomposition, which shows that the PS contents in these two abrasives are 27.16 wt% and 63.55 wt%, respectively. The DTA peak positions for PS@CeO₂ and PS@DND are respectively 299.5 and 360.99 °C. This difference suggests that the content and type of coating material may affect the thermal conductivity of core-shell structured abrasives. TG-DTA results (ESI Fig. S6 and Table S3) for abrasives containing varied coating materials also verified this conclusion. As CeO₂ particles are homogeneously and intensively coated on PS, more efficient heat transfer can be actualized. At the second stage on TG curve of PS@CeO₂, 6.42 wt% of weight lost at ~ 400 °C with the endothermic peak centered at 374.73 °C. This slight and fast process may be resulted from CeO₂ dehydroxylation. Thereafter, there is no more weight-loss, showing that only CeO₂, accounting for 66.42 wt%, was left after removing structural water. The second weight-loss (35.49 wt%) for PS@DND initiated at ~ 480 °C and lasted till ~ 650 °C, with the endothermic peak at 597.07 °C, is caused by carbon oxidation.

As for PS@CeO₂/DND, there are three weight-loss stages and three endothermic peaks. The sequential weight-loss stages with the endothermic peaks centered at 318.78, 400.66 and 578.04 °C are corresponding to PS decomposition (41.29 wt%), CeO₂ dehydroxylation (7.29 wt%) and DND oxidation (27.06 wt%), respectively. After ~ 620 °C, no more change was detected on TG-DTA curves, and the residual CeO₂ accounts for 24.36 wt%.

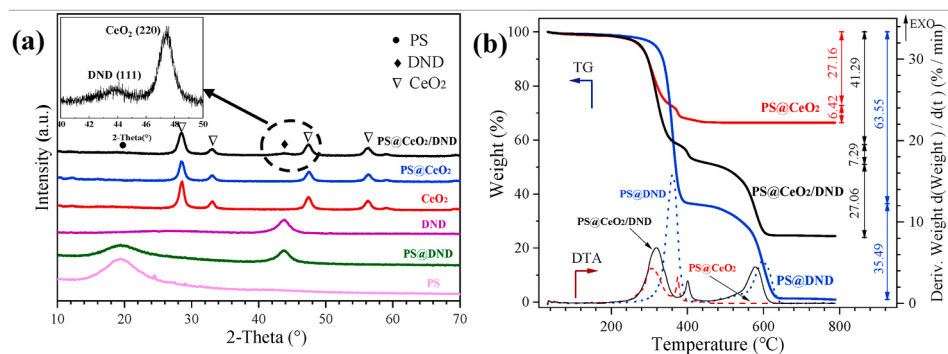


Fig. 3. XRD patterns (a) of PS microspheres, CeO₂, DND, PS@CeO₂, PS@DND and PS@CeO₂/DND and TG-DTA curves (b) of composite abrasives.

3.4. FTIR analysis

Fig. 4(a) shows the FTIR spectra of PS, PS@CeO₂, PS@DND and PS@CeO₂/DND, and the assignment of absorption bands is given in Table 2. Typical bands of phenyl group, C–H out-of-plane bending vibrations (at 700 and 760 cm⁻¹), C=C vibration (1600–1450 cm⁻¹), overtones (2000–1700 cm⁻¹) and C–H stretching vibrations (3000–3100 cm⁻¹) [42] can be clearly observed on FTIR spectrum of PS. C–H stretching vibrations of hydrocarbon chain can also be observed at 3000–2850 cm⁻¹. All these characteristic peaks for PS can be found on FTIR spectra of composite abrasives.

The FTIR spectra of pristine DND, CTAB-modified DND and as-prepared ceria were shown in ESI Fig. S7 and the assignment of absorption bands was listed in ESI Table S4. As there are more hydroxyl groups on CeO₂ and DND particles, the broad absorption peak at ~3400 cm⁻¹ which corresponds to O–H stretching vibration [39], and, as shown in the normalized bands of 1800–1520 cm⁻¹ (Fig. 4(b)), the –OH bending vibration at ~1640 cm⁻¹, were intensified after their solely or combined assembly on PS core. When DND adsorbed on PS, the stretching vibration of carbonyl groups (ν C = O) overlaps the absorption peak of the lowest wavenumber in the four overtones of mono-substituted benzenoid. Besides, shown as well in Fig. 4(b), asymmetric stretching vibrations of carboxylate appeared at the same position of –OH bending vibration (~1640 cm⁻¹) and resulted in a band intensification. The absorption band at 1320 cm⁻¹ was strengthened, which may be attributed to symmetric stretching vibrations of carboxylate. The characteristic peaks for carboxylate can also be observed on the spectrum of CTAB-modified DND (ESI Fig. S7), which may be attributed to

Table 2
Assignment of infrared absorption bands.

Absorption peak position (cm ⁻¹)	Bond type
760, 700	C–H out-of-plane bending vibrations of benzenoid structure (ring torsion) [39,44]
1150	C–O stretching vibrations
1320	symmetric stretching vibrations of carboxylate
1600–1450	C=C vibration (benzene skeleton vibration) [44]
1640	–OH bending vibrations; asymmetric stretching vibrations of carboxylate
1740	C=O stretching vibrations
2000–1700	typical overtones of monosubstituted benzenoid structure [45]
3000–2850	C–H stretching vibrations of hydrocarbon chain [46,47]
3100–3000	C–H stretching vibrations of benzenoid structure [39]
~3420	–OH stretching vibrations

the interaction between carboxyl groups on DND and the ammonium ions.

As shown in ESI Fig. S7, the infrared absorption of CeO₂ over the low wavenumber band (600–400 cm⁻¹) is the strongest on the whole spectrum. On FTIR spectra of PS@CeO₂ and PS@CeO₂/DND, the Ce–O stretching vibration band (425–523 cm⁻¹) [43] can be found, which means that CeO₂ has coated on PS microspheres. As compared in the normalized band (Fig. 4(c)), the absorption of CeO₂ for PS@CeO₂ and PS@CeO₂/DND is remarkably strong, which is characteristic for the composite structure of PS and other oxides [39,44].

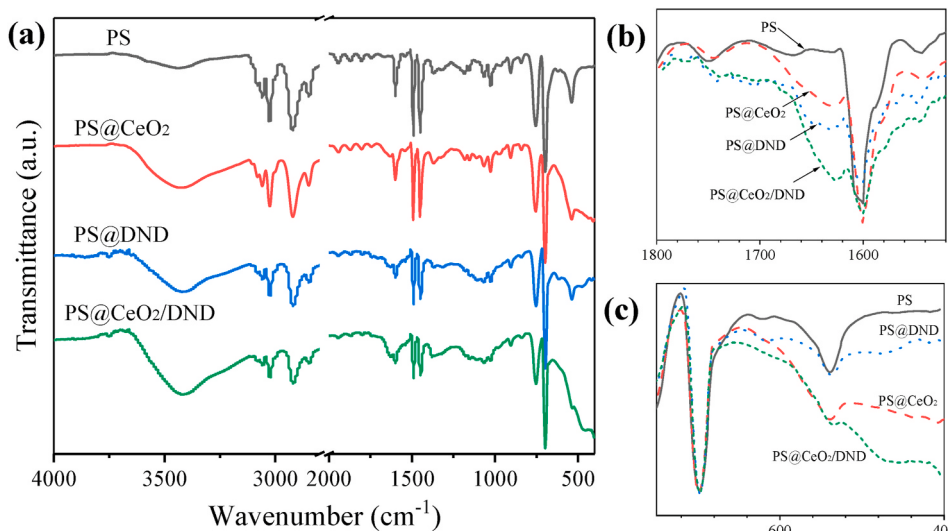


Fig. 4. FTIR spectra of PS microspheres, PS@CeO₂, PS@DND and PS@CeO₂/DND (a), magnified spectra at band 1800–1520 cm⁻¹ (b) and 750–400 cm⁻¹ (c).

3.5. Morphology and composition of composite abrasives

Fig. 5 shows the SEM images in different magnification of composite abrasives and the corresponding EDS spectra were superposed thereon. As shown in **Fig. 5(a)** and **(b)**, PS@CeO₂ composite microspheres are about 500 nm in diameter of spherical appearance. Compared with the morphology of PS colloids (**Fig. 1**), more grainy materials, namely, some bumps and burrs, distributed evenly on PS surface. On its EDS spectrum, the K α radiations of C and O, CK α and OK α , were observed at 0.28 and 0.52 keV, respectively. Meanwhile, CeL radiations including CeL α (4.86 keV), CeL β (5.27 and 5.61 keV) and CeL γ (6.06 and 6.27 keV) and CeM α radiation peak (0.89 keV) can be detected. These peaks are characteristic peaks of CeO₂, which testified that CeO₂ nanoparticles were coated on PS [48–50]. As seen in ESI Table S5, the atomic percentages of Ce and O are 6.09 % and 16.37 %, respectively (Ce:O = 1:2.688), which is in accordance with the stoichiometric ratio of Ce and O elements in CeO₂. The superfluous O may come from the adsorbed oxygenous species.

Compared with PS@CeO₂, the surface morphology of PS@DND is different. As shown in SEM images of PS@DND (**Fig. 5(c)** and **(d)**), PS microspheres were decorated by some particulate matter of irregular morphology. As shown on its EDS spectrum, there are only C (CK α at 0.28 keV) and O (OK α at 0.52 keV) radiation peaks were detected. The atomic percentage of C from both PS and DND accounted for 95.85 % (ESI Table S5), while the small quantity of O elements may be originated

to the functional groups on diamond particles or the adsorbed surfactants. Both the SEM image and the EDS data testified that DND particles have been successfully loaded on PS.

As for the PS@CeO₂/DND abrasives, shown in **Fig. 5(e)** and **(f)**, DND and CeO₂ nanoparticles can be clearly distinguished on PS microspheres. CeO₂ crystallites, which are somewhat homogeneous in size, uniformly distributed on PS, forming a layer with evenly developed thickness. On this CeO₂ coating attached unevenly small DND clusters. Compared with PS@CeO₂, the surface of PS@DND and PS@CeO₂/DND abrasives are rougher, which may attribute to the irregular-shaped DND clusters. The radiations of O, Ce appeared as well on its EDS spectrum. The percentage of Ce declined slightly, while that of O ascended (ESI Table S5), which may suggest that more oxygen-containing groups existed on PS@CeO₂/DND.

TEM images of these composite abrasives are presented in **Fig. 6**. It can be seen from **Fig. 6(a)** and **(b)** that, on the periphery of PS@CeO₂, the shell is composed of a large number of ceria nanoparticles. As shown in the HRTEM image (**Fig. 6(c)**), the ceria particles, with the size of around 10 nm, are of regular cubic-structure. According to the lattice structure of a crystallite, the space between two adjacent lattice fringes is about 0.31 nm, which corresponds to the (111) lattice plane of cubic ceria. **Fig. 6(d)** and **(e)** show that PS microspheres are covered by a DND layer and the size of composites was about 500 nm. Compared with PS and PS@CeO₂, PS@DND particles exhibit a rougher appearance. It can

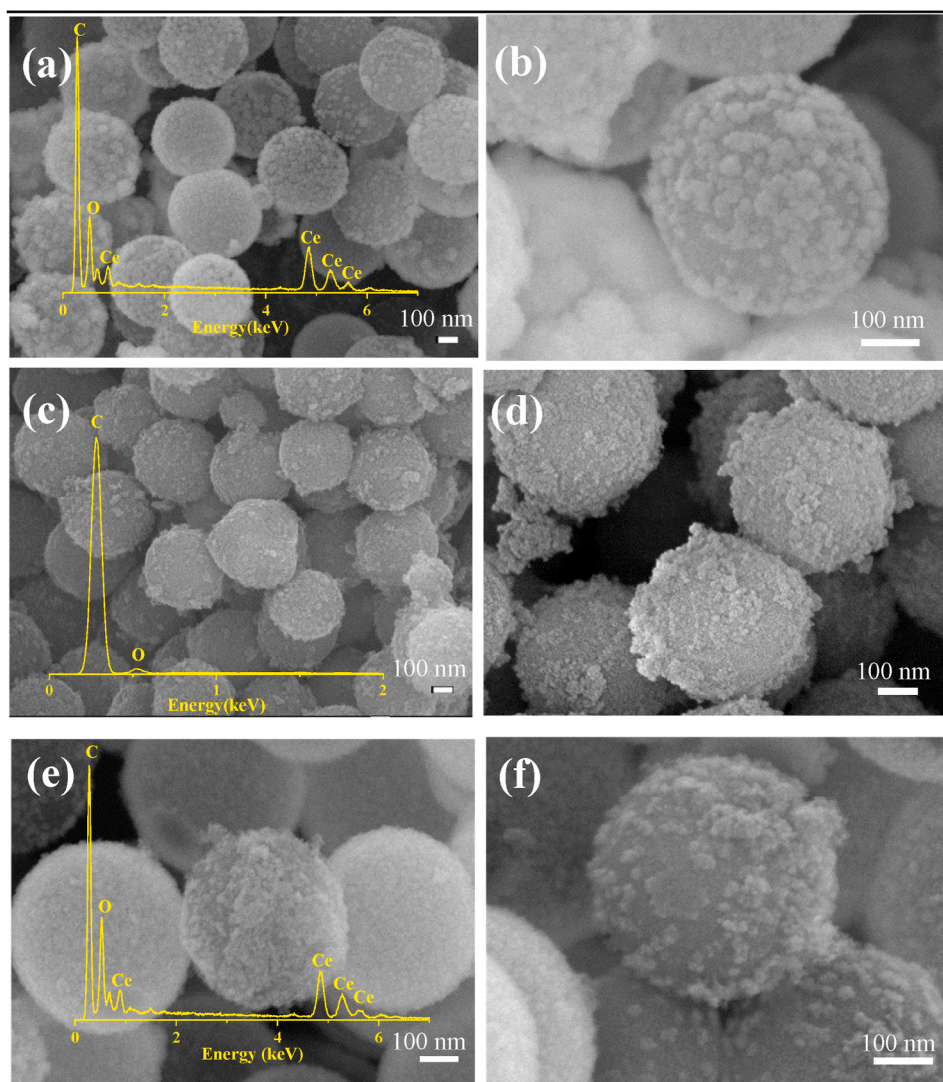


Fig. 5. SEM images of PS@CeO₂ (a, b), PS@DND (c, d), PS@CeO₂/DND (e, f) abrasive particles.

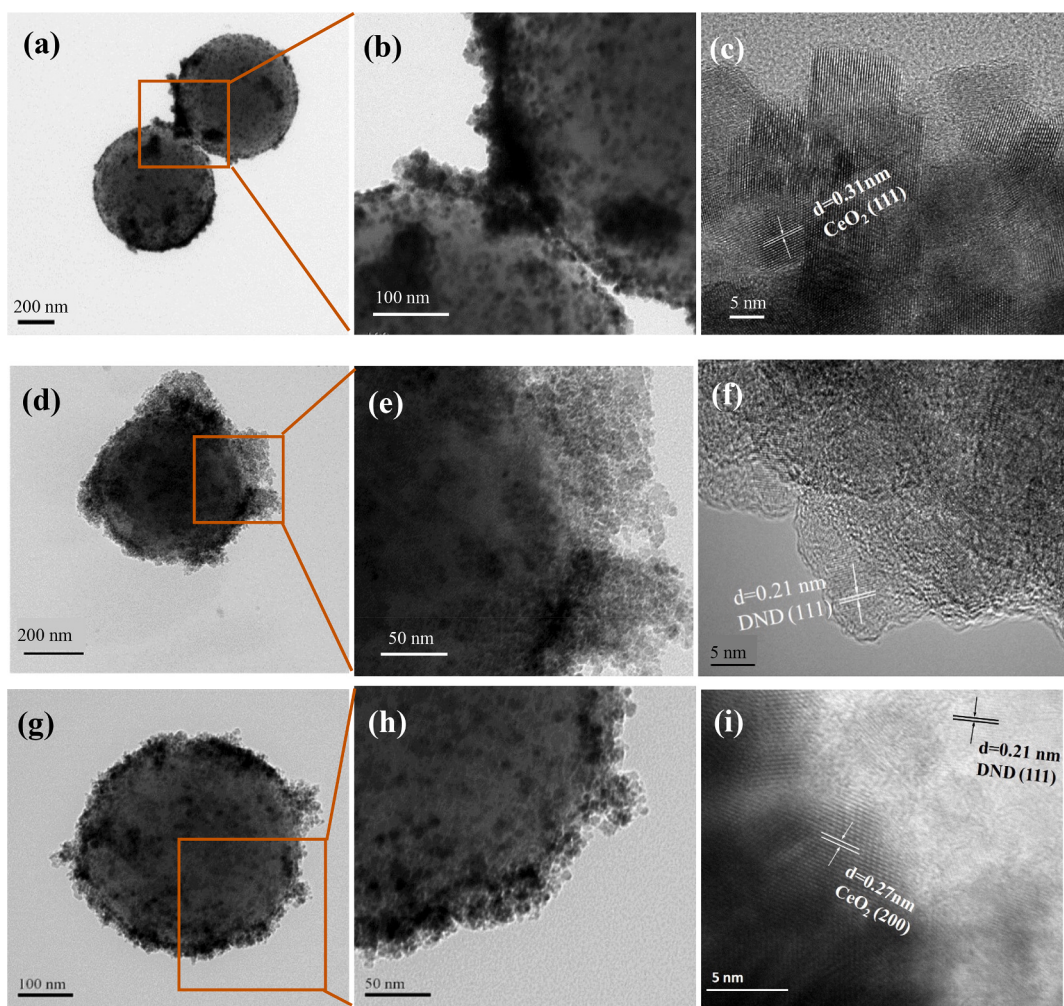


Fig. 6. TEM images of PS@CeO₂ (a, b and c), PS@DND (d, e and f), PS@CeO₂/DND (g, h and i) abrasive particles.

be seen from Fig. 6(f) that DND clusters on PS are composed by round-shaped crystallites of ~5 nm in diameter and the interplanar distance calculated to be ~0.21 nm, which corresponds to the (111) lattice plane of diamond. Fig. 6(g) and (h) show the typical TEM images of a PS@CeO₂/DND composite particle. The abrasive is of globular structure and there are some bright and dark areas thereon. As ceria has stronger electron scattering, the dark and well-dispersed granules are CeO₂ nanoparticles while the particles on the brink, with lightish color and irregular shape, are small DND clusters. As shown in Fig. 6(i), lattice structures for both ceria and diamond can be measured, which verifies

the combined deposition of these two kinds of particles.

3.6. Polishing performance

CMP is a quite complex technology and the polishing performance may be affected by many factors [51]. As shown in Fig. 7(a), MRR ascends along with the increase of rotating speed. When the rotating speed rises to ~120 rpm, the MRR increasing rate slows down. This gradual increase of MRR may be attributed to the activation energy strengthened via interface friction. However, owing to the increase of centrifugal force

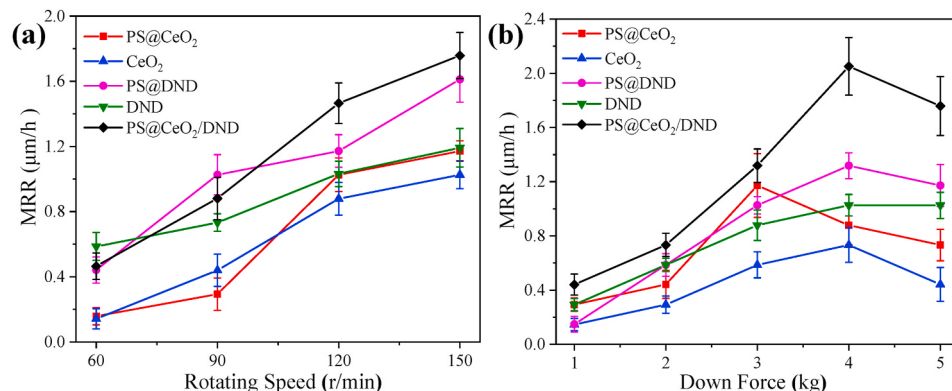


Fig. 7. Influence of rotating speed (a) and down force (b) on MRR obtained by using different abrasive.

by speeding up platen rotating, the retention time for abrasives on polishing pad was shortened. As the participation of abrasives in polishing operation was restricted, it is hard to increase further MRR by an accelerating approach. At a rotating speed of 150 rpm, MRR for PS@CeO₂, PS@DND and PS@CeO₂/DND reached 1.2, 1.6 and 1.7 $\mu\text{m h}^{-1}$, respectively. It is obvious that, the MRR for composite abrasives is generally 10–20 % higher than that for unitary abrasives, especially at higher rotating speed. This may be attributed to the reducing of centrifugal force and the increase of viscous force contributed by the elastic and low-density composites [32].

Down force also plays a crucial role in the polishing performance (Fig. 7(b)). On each MRR-down force curve, there is a climax MRR value for unitary abrasives and the composited ones when the loaded force is around 4 kg. The highest MRR values for PS@CeO₂, PS@DND and PS@CeO₂/DND amount up to 1.17, 1.61 and 2.05 $\mu\text{m h}^{-1}$, respectively. It can be concluded that, owing to the mechanical polishing effect of superhard particles, the MRR value for DND coated PS can be remarkably upgraded. Because of the combined effect of ceria and DND, PS@CeO₂/DND owns even higher MRR.

This difference may be explained by the change of contacting area. For free CeO₂ and DND abrasives, owing to the diversity in size and morphology, only a few particles contributed in the polishing process. The inert small particles may result in a reduction of the total actual contacting area. As for the elastic composite abrasives, a deformation can easily occur under the same load, which can sustain large effective contacting interface and ensure the polishing efficiency [37,52]. Meanwhile, the abrasive particles fixed on PS are much denser than the free abrasives, the polishing capacity can be improved [53].

As shown in the digital photos (ESI Fig. S8) and SEM images (ESI

Fig. S9), the white matt surface was lapped to a mirror finish after polished by composite abrasives. AFM image of unpolished sapphire wafer (Fig. 8(a)) testified its rough surface ($\text{Ra} = 3.23 \text{ nm}$), while deep ravines and machining defects thereon are obvious. As can be seen from the typical AFM image of wafers polished by CeO₂ (Fig. 8(b)) and DND (Fig. 8(c)), the topography fluctuation of sapphire surface is smoothed, while the Ra value was decreased respectively to 1.38 and 1.29 nm. But there are still some bumps and scratches. Fig. 8(d)–(f) show AFM images of sapphire surface polished by PS@CeO₂, PS@DND and PS@CeO₂/DND.

Compared with raw sapphire and those processed by unitary abrasives, wafers polished by composite abrasives exhibit decreased Ra and declined topographical variations, and the scratches have almost vanished. This is in accordance with other research on composite abrasives, which concluded that, as the core-shell abrasives were increased in diameter, the clearance between wafer and pad can be widened which benefits the removal of by-products and the diminution of scratch derivation [53]. The Ra of sapphire polished by PS@CeO₂, PS@DND and PS@CeO₂/DND abrasives are respectively 1.25, 0.63 and 0.52 nm.

As showed in Fig. 8(f), the surface quality of sapphire treated by PS@CeO₂/DND abrasives is superior to those polished by other abrasives. The ternary composite particles can eliminate effectively surface defects as bumps, scratches and residual particles can hardly be observed on PS@CeO₂/DND polished surface. As shown in ESI Table S6, the Ra values for sapphire wafers polished by these composite abrasives are superior to those obtained using silica-based or alumina-based abrasives.

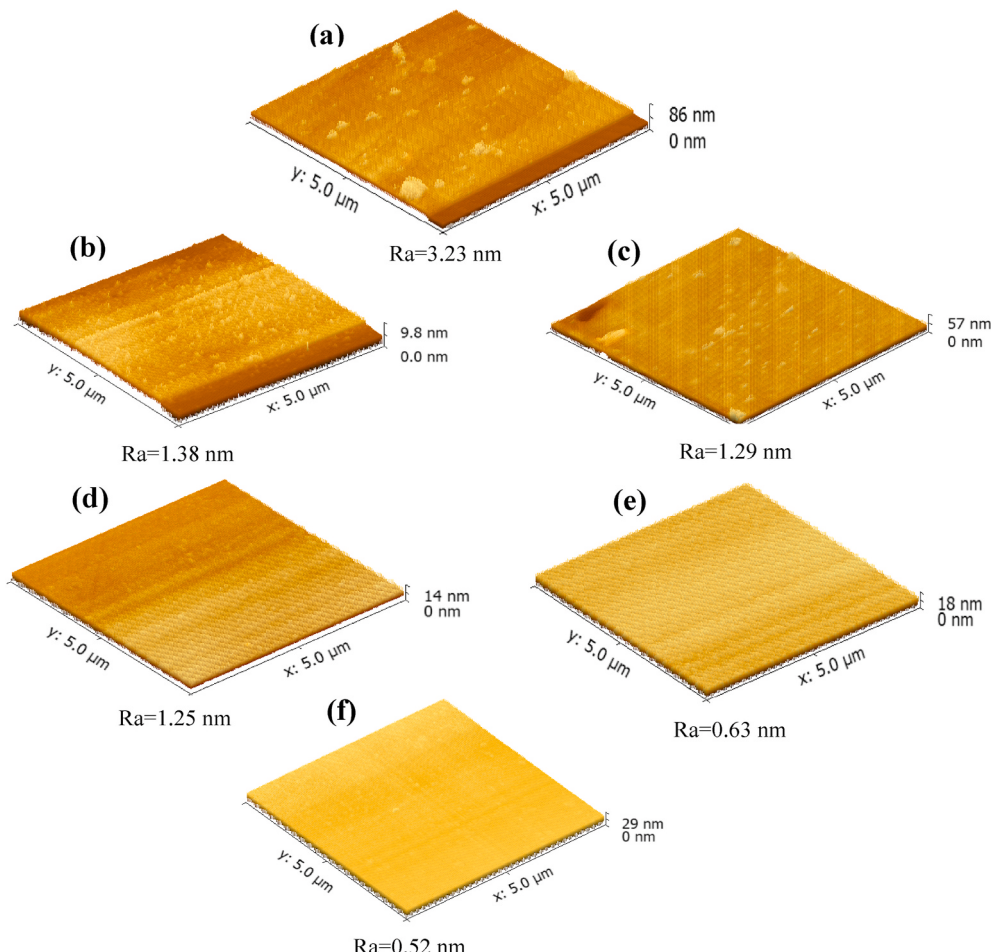


Fig. 8. AFM images of sapphire surface for unpolished sample (a) and samples polished by CeO₂ (b), DND (c), PS@CeO₂ (d), PS@DND (e) and PS@CeO₂/DND (f).

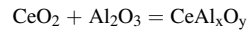
3.7. Polishing mechanism

The slurry collected from the PS@CeO₂/DND polishing process was dried for XPS analysis. Fig. 9 shows its C1s, O1s, Al2p and Ce3d XPS narrow scan spectra.

It can be concluded from the deconvolution peaks of C1s XPS narrow scan spectrum that, there are mainly four chemical states of C element in the detritus. The peak at 284.4 eV, corresponding to the C-C bonding for the hydrocarbon groups, can be attributed to the PS structure in composite abrasives [54]. The peak centered at 285.3 eV corresponds to DND component [55], while peaks at 286.2 eV and 287.1 eV can be attributed to the C=O and C=O/C-OH species [56].

The lower binding energy (BE) peaks on O1s spectrum can be attributed to metal oxides such as CeO₂ (529.4 eV) [57] and Al₂O₃ (530.3 eV), while the peak at 531.9 eV corresponds to AlOOH [11]. The peaks at 531.1 eV and 532.9 eV can be attributed to C=O/C-OH [58] and C=O species [55].

On Al2p spectrum, the BE peaks at 75.0 eV, 74.2 eV and 73.2 eV correspond to the chemical states of Al₂O₃ [59], Al(OH)₃ [60] and AlOOH [59], respectively. It proves that some sapphire detritus (Al₂O₃) were polished down and there existed chemical reactions on the wafer in the alkaline slurry which derived AlOOH and Al(OH)₃ (Eqs. (2) and (3)) [5,9,11–13,24]. In addition, the BE peak centered at 71.9 eV may correspond to CeAl_xO_y (Eq. (4)), the compounding formation of ceria and alumina, which resulted from the chemical mechanical reaction of ceria particles on sapphire.



The BE peaks (882.88 (v₀), 888.76 (v'), 901.03 (u₀) and 907.57 eV (u')) on Ce 3d spectrum correspond to Ce³⁺ chemical states, while other peaks correspond to Ce⁴⁺ [61], which may be related to the formation of CeAl_xO_y.

As a typical CMP abrasive, CeO₂ can remove, at the initial stage of polishing, the bump layer on sapphire and expose fresh surface. Meanwhile, on sapphire with the main component as Al₂O₃, a surface erosion and hydrolyzation initiated and developed along with the polishing process. Then, as there generates an aluminate gel layer on sapphire, the surface is softened and can be efficiently abraded with DND particles. Compared with single abrasives, composite particles exhibit non-rigid mechanical properties and the inorganic shells stiffened the organic cores. As what has been schematically illustrated in the microcontact models [4,20,53,62], the elastic deformation of organic cores and denser distribution of abrasive particles may increase the abrasive-wafer contact area. During CMP, the contact stress and the indentation depth of abrasive onto sapphire were decreased [4,20,53], which helps to reduce mechanical damage and the wafer can be polished to sub-nanoscale. Moreover, coated by CeO₂ and DND carrying abundant hydrophilic groups, PS microspheres can easily disperse and then maintain stable in aqueous media. Composite abrasives can evenly distribute onto the carrier, which can improve their polishing performance. It's because the combined polishing functions of the hybrid coating composing of superhard nanoscaled diamond particles and chemically active abrasive CeO₂, and the elastic characteristic provided by the backup from PS core, excellent mechanical and chemical polishing capacity can be achieved by PS@CeO₂/DND.

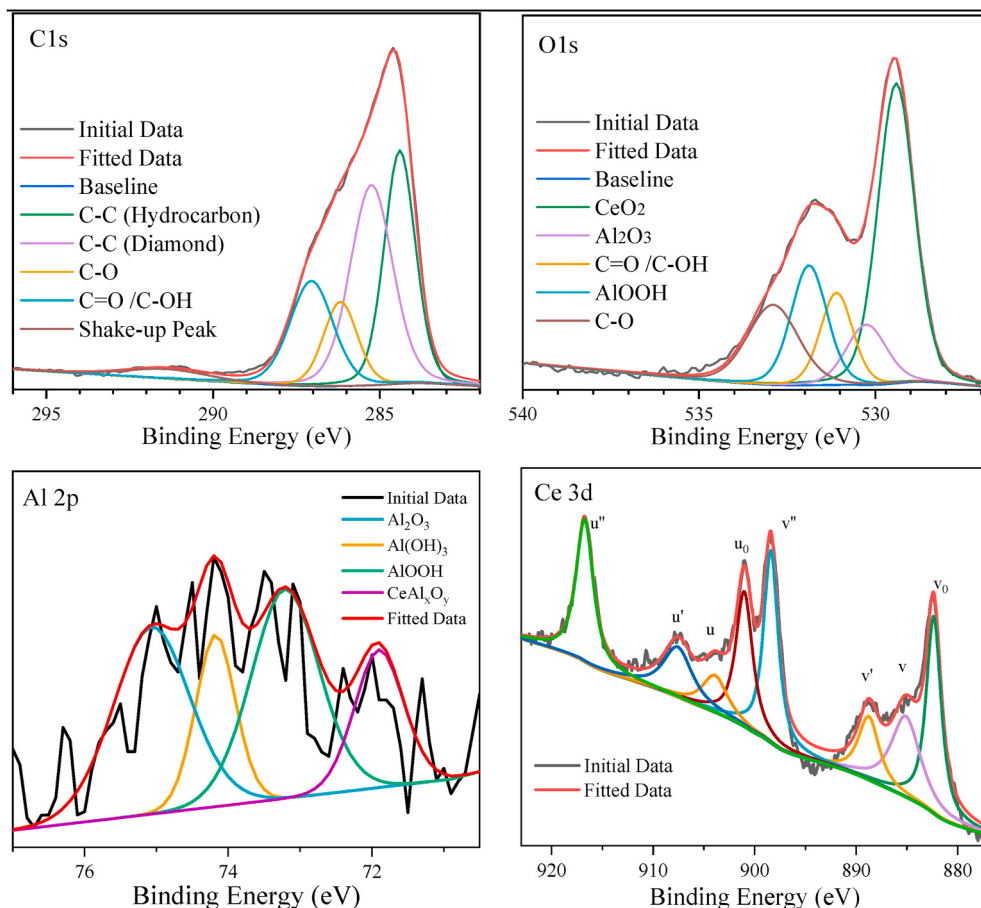


Fig. 9. C1s, O1s, Al2p and Ce3d XPS narrow scan spectra for polished detritus.

4. Conclusions

By depositing CeO₂ or/and DND particles on PS colloids, core-shell structured abrasives can be facilely synthesized. In these abrasives, the PS cores are of regular spherical shape with a mean size of around 400 nm and CeO₂ or/and DND attached and evenly distributed thereon forms out layer of ~50 nm thick. The mechanism for the self-assembly of composite abrasives is the electrostatic attraction between negatively charged PS colloids and cerium cations or/and positively charged DND particles. The composite abrasives exhibited excellent performance on sapphire CMP processing. The MRR values of sapphires polished by composite abrasives were 10–20 % higher than those by their unitary counterparts. Compared to sapphire wafers polished by CeO₂ (Ra = 1.38 nm) and DND (Ra = 1.29 nm), Ra values for composite abrasive polished ones were significantly reduced. After polished using ternary abrasive, PS@CeO₂/DND, the sapphire surface can be smoothed to a sub-nanoscale roughness (Ra = 0.52 nm). The improved CMP efficiency can be attributed to the synergistic effect of organic cores and inorganic shells. The elastic PS spheres may help to increase the polishing duration and the effective contacting interface, while densely distributed CeO₂ and DND particles can perform actively in a combined polishing operation. The improved polishing performance may as well be attributed to both the chemical erosion of CeO₂ on wafer surface and the intensive mechanical removal of DND.

Declaration of competing interest

The authors declare that they have no conflict of interests or personal relationships that could have appeared to influence the work reported in this paper.

Acknowledgements

This work was supported by the Opening Project of Hunan Key Laboratory of Mineral Materials and Application (MMA201701) and by the Open-End Fund for Laboratory Research of Central South University (512110001). We appreciate the kind help from Sichuan Xintong New Material Co., Ltd. and Chengdu Fortune Myriad Diamond Nano-Tech Co., Ltd. for providing free sapphire wafers and DND powder samples.

Appendix A. Supplementary data

Supplementary data to this article can be found online at <https://doi.org/10.1016/j.ceramint.2021.08.048>.

References

- [1] C.P. Khattak, R. Shetty, C.R. Schwerdtfeger, S. Ullal, World's largest sapphire for many applications, *J. Cryst. Growth* 452 (2016) 44–48, <https://doi.org/10.1016/j.jcrysgro.2015.11.026>.
- [2] M. Bhattacharya, A. Dey, A.K. Mukhopadhyay, Influence of loading rate on nanohardness of sapphire, *Ceram. Int.* 42 (2016) 13378–13386, <https://doi.org/10.1016/j.ceramint.2016.05.091>.
- [3] J. Wang, B. Guo, Q. Zhao, C. Zhang, Q. Zhang, W. Zhai, Evolution of material removal modes of sapphire under varied scratching depths, *Ceram. Int.* 43 (2017) 10353–10360, <https://doi.org/10.1016/j.ceramint.2017.05.069>.
- [4] T. Wang, H. Lei, Novel polyelectrolyte-Al₂O₃/SiO₂ composite nanoabrasives for improved chemical mechanical polishing (CMP) of sapphire, *J. Mater. Res.* 34 (2019) 1073–1082, <https://doi.org/10.1557/jmr.2018.443>.
- [5] H. Lee, H. Lee, H. Jeong, S. Choi, Y. Lee, M. Jeong, H. Jeong, Macroscopic and microscopic investigation on chemical mechanical polishing of sapphire wafer, *J. Nanosci. Nanotechnol.* 12 (2012) 1256–1259, <https://doi.org/10.1166/jnn.2012.4679>.
- [6] L. Xu, C. Zou, X. Shi, G. Pan, G. Luo, Y. Zhou, Fe-N_x/C assisted chemical-mechanical polishing for improving the removal rate of sapphire, *Appl. Surf. Sci.* 343 (2015) 115–120, <https://doi.org/10.1016/j.apsusc.2015.03.041>.
- [7] E.A. Vovk, A.T. Budnikov, M.V. Dobrotvorskaya, S.I. Krivonogov, A.Y. Dan'ko, Mechanism of the interaction between Al₂O₃ and SiO₂ during the chemical-mechanical polishing of sapphire with silicon dioxide, *J. Surf. Invest.: X-Ray, Synchrotron Neutron Tech* 6 (2012) 115–121, <https://doi.org/10.1134/S1027451012020188>.
- [8] A. Montagne, S. Pathak, X. Maeder, J. Michler, Plasticity and fracture of sapphire at room temperature: load-controlled microcompression of four different orientations, *Ceram. Int.* 40 (2014) 2083–2090, <https://doi.org/10.1016/j.ceramint.2013.07.121>.
- [9] H. Lei, K. Tong, Z. Wang, Preparation of Ce-doped colloidal SiO₂ composite abrasives and their chemical mechanical polishing behavior on sapphire substrates, *Mater. Chem. Phys.* 172 (2016) 26–31, <https://doi.org/10.1016/j.matchemphys.2015.12.026>.
- [10] P. Ma, H. Lei, Y. Chen, Preparation of Ni-doped colloidal silica abrasives and their chemical mechanical polishing performances on sapphire, *ECS J. Solid State Sci. Technol.* 5 (2016) Q132–Q136, <https://doi.org/10.1149/2.0221605jss>.
- [11] W. Xie, Z. Zhang, L. Liao, J. Liu, H. Su, S. Wang, D. Guo, Green chemical mechanical polishing of sapphire wafers using a novel slurry, *Nanoscale* 12 (2020) 22518–22526, <https://doi.org/10.1039/DONR04705H>.
- [12] H. Lei, T. Liu, L. Xu, Synthesis of Sm-doped colloidal SiO₂ composite abrasives and their chemical mechanical polishing performances on sapphire substrates, *Mater. Chem. Phys.* 237 (2019) 121819, <https://doi.org/10.1016/j.matchemphys.2019.121819>.
- [13] T. Liu, H. Lei, Nd³⁺-doped colloidal SiO₂ composite abrasives: synthesis and the effects on chemical mechanical polishing (CMP) performances of sapphire wafers, *Appl. Surf. Sci.* 413 (2017) 16–26, <https://doi.org/10.1016/j.apsusc.2017.03.270>.
- [14] Y. Zhou, G. Pan, H. Gong, X. Shi, C. Zou, Characterization of sapphire chemical mechanical polishing performances using silica with different sizes and their removal mechanisms, *Colloids Surf., A* 513 (2017) 153–159, <https://doi.org/10.1016/j.colsurfa.2016.09.049>.
- [15] Y. Zhou, G. Pan, X. Shi, S. Zhang, H. Gong, G. Luo, Effects of ultra-smooth surface atomic step morphology on chemical mechanical polishing (CMP) performances of sapphire and SiC wafers, *Tribol. Int.* 87 (2015) 145–150, <https://doi.org/10.1016/j.tribon.2015.02.013>.
- [16] Z. Zhang, W. Zhang, S. Zhang, W. Yan, Study on chemical mechanical polishing performances of sapphire wafer (0001) using silica-based slurry, *ECS J. Solid State Sci. Technol.* 6 (2017) P723–P727, <https://doi.org/10.1039/DONR04705H>.
- [17] X. Liu, X. Xu, Ultra-fine polishing of glass-ceramics by disaggregated and fractionated detonation nanodiamond, *Ceram. Int.* 43 (2017) 6063–6068, <https://doi.org/10.1016/j.ceramint.2017.01.150>.
- [18] J. Lu, Y. Wang, Q. Luo, X. Xu, Photocatalysis assisting the mechanical polishing of a single-crystal SiC wafer utilizing an anatase TiO₂-coated diamond abrasive, *Precis. Eng.* 49 (2017) 235–242, <https://doi.org/10.1016/j.precisioneng.2017.02.011>.
- [19] Z. Zhang, L. Yu, W. Liu, Z. Song, Surface modification of ceria nanoparticles and their chemical mechanical polishing behavior on glass substrate, *Appl. Surf. Sci.* 256 (2010) 3856–3861, <https://doi.org/10.1016/j.apsusc.2010.01.040>.
- [20] X. Wang, H. Lei, R. Chen, CMP behavior of alumina/metatitanic acid core-shell abrasives on sapphire substrates, *Precis. Eng.* 50 (2017) 263–268, <https://doi.org/10.1016/j.precisioneng.2017.05.013>.
- [21] X. Shi, L. Xu, Y. Zhou, C. Zou, R. Wang, G. Pan, An in situ study of chemical-mechanical polishing behaviours on sapphire (0001) via simulating the chemical product-removal process by AFM-tapping mode in both liquid and air environments, *Nanoscale* 10 (2018) 19692–19700, <https://doi.org/10.1039/C8NR04645J>.
- [22] X. Zhao, R. Long, Y. Chen, Z. Chen, Synthesis, characterization of CeO₂@SiO₂ nanoparticles and their oxide CMP behavior, *Microelectron. Eng.* 87 (2010) 1716–1720, <https://doi.org/10.1016/j.mee.2009.09.012>.
- [23] H. Lei, L. Huang, Q. Gu, Synthesis of Zn-doped colloidal SiO₂ abrasives and their applications in sapphire chemical mechanical polishing slurry, *J. Mater. Sci. Mater. Electron.* 28 (2016) 1229–1237, <https://doi.org/10.1007/s10854-016-5650-7>.
- [24] Z. Zhang, J. Liu, W. Hu, L. Zhang, W. Xie, L. Liao, Chemical mechanical polishing for sapphire wafers using a developed slurry, *J. Manuf. Process.* 62 (2021) 762–771, <https://doi.org/10.1016/j.jmapro.2021.01.004>.
- [25] Z. Zhang, J. Cui, J. Zhang, D. Liu, Z. Yu, D. Guo, Environment friendly chemical mechanical polishing of copper, *Appl. Surf. Sci.* 467–468 (2019) 5–11, <https://doi.org/10.1016/j.apsusc.2018.10.133>.
- [26] Z. Zhang, L. Liao, X. Wang, W. Xie, D. Guo, Development of a novel chemical mechanical polishing slurry and its polishing mechanisms on a nickel alloy, *Appl. Surf. Sci.* 506 (2020) 144670, <https://doi.org/10.1016/j.apsusc.2019.144670>.
- [27] Z. Zhang, B. Wang, P. Zhou, R. Kang, B. Zhang, D. Guo, A novel approach of chemical mechanical polishing for cadmium zinc telluride wafers, *Sci. Rep. -UK* 6 (2016) 26891, <https://doi.org/10.1038/srep26891>.
- [28] L. Liao, Z. Zhang, F. Meng, D. Liu, B. Wu, Y. Li, W. Xie, A novel slurry for chemical mechanical polishing of single crystal diamond, *Appl. Surf. Sci.* 564 (2021) 150431, <https://doi.org/10.1016/j.apsusc.2021.150431>.
- [29] H. Lei, L. Jiang, R. Chen, Preparation of copper-incorporated mesoporous alumina abrasive and its CMP behavior on hard disk substrate, *Powder Technol.* 219 (2012) 99–104, <https://doi.org/10.1016/j.powtec.2011.12.022>.
- [30] L. Liao, Z. Zhang, F. Meng, D. Liu, J. Liu, Y. Li, X. Cui, Novel rotary chemical mechanical polishing on an integral impeller, *J. Manuf. Process.* 66 (2021) 198–210, <https://doi.org/10.1016/j.jmapro.2021.04.010>.
- [31] H. Chunman, J.C. Yu, T. Kwong, A.C. Mak, S. Lai, Morphology-controllable synthesis of mesoporous CeO₂ nano- and microstructures, *Chem. Mater.* 17 (2005) 4514–4522, <https://doi.org/10.1021/cm0507967>.
- [32] L. Zhang, H. Wang, Z. Zhang, F. Qin, W. Liu, Z. Song, Preparation of monodisperse polystyrene/silica core-shell nano-composite abrasive with controllable size and its chemical mechanical polishing performance on copper, *Appl. Surf. Sci.* 258 (2011) 1217–1224, <https://doi.org/10.1016/j.apsusc.2011.09.074>.
- [33] S. Armini, C.M. Whelan, K. Maex, J.L. Hernandez, M. Moinpour, Composite polymer-core silica-shell abrasives particles during oxide CMP, *J. Electrochem. Soc.* 154 (2007) H667–H671, <https://doi.org/10.1149/1.2740038>.

- [34] Y. Chen, Z. Li, N. Miao, Synergetic effect of organic cores and inorganic shells for core/shell structured composite abrasives for chemical mechanical planarization, *Appl. Surf. Sci.* 314 (2014) 180–187, <https://doi.org/10.1016/j.apsusc.2014.06.166>.
- [35] A. Chen, Y. Wang, J. QINin, Z. Li, Chemical mechanical polishing for SiO₂ film using polystyrene@ceria (PS@CeO₂) core-shell nanocomposites, *J. Inorg. Organomet. Polym.* 25 (2015) 1407–1413, <https://doi.org/10.1007/s10904-015-0253-y>.
- [36] Y. Chen, R. Long, Polishing behavior of PS/CeO₂ hybrid microspheres with controlled shell thickness on silicon dioxide CMP, *Appl. Surf. Sci.* 257 (2011) 8679–8685, <https://doi.org/10.1016/j.apsusc.2011.05.047>.
- [37] Y. Chen, Z. Li, N. Miao, Polymethylmethacrylate (PMMA)/CeO₂ hybrid particles for enhanced chemical mechanical polishing performance, *Tribol. Int.* 82 (2015) 211–217, <https://doi.org/10.1016/j.triboint.2014.10.013>.
- [38] Y. Chen, J. Qin, Y. Wang, Z. Li, Core/shell composites with polystyrene cores and meso-silica shells as abrasives for improved chemical mechanical polishing behavior, *J. Nano Res.* 17 (2015) 363, <https://doi.org/10.1007/s11051-015-3172-5>.
- [39] F. Shi, Y. Li, H. Wang, Q. Zhang, Formation of core/shell structured polystyrene/anatase TiO₂ photocatalyst via vapor phase hydrolysis, *Appl. Catal., B* 123–124 (2012) 127–133, <https://doi.org/10.1016/j.apcatb.2012.04.032>.
- [40] W. Wang, Y. Jiang, S. Wen, L. Liu, L. Zhang, Preparation and characterization of polystyrene/Ag core-shell microspheres - a bio-inspired poly(dopamine) approach, *J. Colloid Interface Sci.* 368 (2012) 241–249, <https://doi.org/10.1016/j.jcis.2011.10.047>.
- [41] Z. Yang, Y. Yang, H. Liang, L. Liu, Hydrothermal synthesis of monodisperse CeO₂ nanocubes, *Mater. Lett.* 63 (2009) 1774–1777, <https://doi.org/10.1016/j.matlet.2009.05.034>.
- [42] Y. Chen, J. Lu, Z. Chen, Preparation, characterization and oxide CMP performance of composite polystyrene-core ceria-shell abrasives, *Microelectron. Eng.* 88 (2011) 200–205, <https://doi.org/10.1016/j.mee.2010.10.019>.
- [43] B. Ksapabutr, E. Gulari, S. Wongkasemjai, Sol-gel derived porous ceria powders using cerium glycolate complex as precursor, *Mater. Chem. Phys.* 99 (2006) 318–324, <https://doi.org/10.1016/j.matchemphys.2005.10.030>.
- [44] A. Angelopoulou, E.K. Efthimiadou, N. Boukos, G. Kordas, A new approach for the one-step synthesis of bioactive PS vs. PMMA silica hybrid microspheres as potential drug delivery systems, *Colloids Surf., B* 117 (2014) 322–329, <https://doi.org/10.1016/j.colsurfb.2014.02.047>.
- [45] W. Wang, Y. Deng, L. Zhang, J. Fu, Z. Lu, L. Xu, Preparation and characterization of polystyrene microspheres in the presence of β-cyclodextrin, *J. Nanosci. Nanotechnol.* 12 (2012) 7206–7210, <https://doi.org/10.1166/jnn.2012.6504>.
- [46] I.A. Kartsonakis, P. Liatsi, I. Daniilidis, G. Kordas, Synthesis, characterization, and antibacterial action of hollow ceria nanospheres with/without a conductive polymer coating, *J. Am. Ceram. Soc.* 91 (2008) 372–378, <https://doi.org/10.1111/j.1551-2916.2007.02088.x>.
- [47] X. Wang, Y. Zhang, F. Lv, B. Shen, R. Zhang, F. Zhou, P.K. Chu, Cross-linked polystyrene microspheres as density-reducing agent in drilling fluid, *J. Petrol. Sci. Eng.* 78 (2011) 529–533, <https://doi.org/10.1016/j.petrol.2011.06.016>.
- [48] F. Gao, Z. Xu, Q. Wang, Z. Hu, G. Gu, Preparation, characterization of CeO₂-ZrO₂ composite hollow microspheres and their application as electrocatalysis materials for hemoglobin in biosensor, *J. Dispersion Sci. Technol.* 30 (2009) 178–184, <https://doi.org/10.1080/01932690802498153>.
- [49] Z. Hashemzaei, M. Shariftabar, H. Saravani, M. Noroozifar, Synthesis of porous Mg-doped CeO₂ powders via self-propagating high-temperature synthesis route, *Adv. Powder Technol.* 30 (2019) 2947–2956, <https://doi.org/10.1016/j.apt.2019.09.002>.
- [50] D.V. Rao, R. Cesareo, G.E. Gigante, L α Ll, L β and L γ X-ray fluorescence cross-sections for Ce, Pr and Sm excited by Y and Mo K α X-ray photons, *X Ray Spectrom.* 25 (1996) 74–77, [https://doi.org/10.1002/\(SICI\)1097-4539\(199603\)25:2<74::AID-XRS143>3.0.CO;2-3](https://doi.org/10.1002/(SICI)1097-4539(199603)25:2<74::AID-XRS143>3.0.CO;2-3).
- [51] W. Xu, Y. Cheng, M. Zhong, Effects of process parameters on chemical-mechanical interactions during sapphire polishing, *Microelectron. Eng.* 216 (2019) 111029, <https://doi.org/10.1016/j.mee.2019.111029>.
- [52] Y. Chen, Z. Li, N. Miao, Synergetic effect of organic cores and inorganic shells for core/shell structured composite abrasives for chemical mechanical planarization, *Appl. Surf. Sci.* 314 (2014) 180–187, <https://doi.org/10.1016/j.apsusc.2014.06.166>.
- [53] Y. Huang, X. Xu, C. Yao, J. Hu, W. Peng, Preparation of composite abrasives by electrostatic self-assembly method and its polishing properties in Cu CMP, *Eng. Sci.* 12 (2014) 75–82, <https://doi.org/10.3969/j.issn.1672-4178.2014.02.013>.
- [54] M. Delcroix, E. Zuyderhoff, M. Genet, C. Dupont-Gillain, Optimization of cryo-XPS analyses for the study of thin films of a block copolymer (PS-PEO), *Surf. Interface Anal.* 44 (2012) 175–184, <https://doi.org/10.1002/sia.3793>.
- [55] Y.M. Hunge, A.A. Yadav, S. Khan, K. Takagi, N. Suzuki, K. Teshima, C. Terashima, A. Fujishima, Photocatalytic degradation of bisphenol A using titanium dioxide@nanodiamond composites under UV light illumination, *J. Colloid Interface Sci.* 582 (2021) 1058–1066, <https://doi.org/10.1016/j.jcis.2020.08.102>.
- [56] M. Varge, T. Izak, V. Vretenar, H. Kozak, J. Holovsky, A. Artemenko, M. Hulman, V. Skakalova, D.S. Lee, A. Kromka, Diamond/carbon nanotube composites: Raman, FTIR and XPS spectroscopic studies, *Carbon* 111 (2017) 54–61, <https://doi.org/10.1016/j.carbon.2016.09.064>.
- [57] I. Avramova, S. Suzer, D. Guergova, D. Stoychev, P. Stefanov, CeO_x/Al₂O₃ thin films on stainless steel substrate - dynamical X-ray photoelectron spectroscopy investigations, *Thin Solid Films* 536 (2013) 63–67, <https://doi.org/10.1016/j.tsf.2013.03.049>.
- [58] Y. Kim, D. Lee, S.Y. Kim, E. Kang, C.K. Kim, Nanocomposite synthesis of nanodiamond and molybdenum disulfide, *Nanomaterials* 9 (2019) 927, <https://doi.org/10.3390/nano9070927>.
- [59] Y. Dong, H. Lei, W. Liu, T. Wang, L. Xu, Preparation of non-spherical silica composite abrasives by lanthanum ion-induced effect and its chemical-mechanical polishing properties on sapphire substrates, *J. Mater. Sci.* 53 (2018) 10732–10742, <https://doi.org/10.1007/s10853-018-2357-6>.
- [60] D. Yin, X. Niu, K. Zhang, J. Wang, Y. Cui, Preparation of MgO doped colloidal SiO₂ abrasive and their chemical mechanical polishing performance on c-, r- and a-plane sapphire substrate, *Ceram. Int.* 44 (2018) 14631–14637, <https://doi.org/10.1016/j.ceramint.2018.05.087>.
- [61] C. Anandan, P. Bera, XPS studies on the interaction of CeO₂ with silicon in magnetron sputtered CeO₂ thin films on Si and Si₃N₄ substrates, *Appl. Surf. Sci.* 283 (2013) 297–303, <https://doi.org/10.1016/j.apsusc.2013.06.104>.
- [62] S. Dai, H. Lei, J. Fu, Preparation of SiC/SiO₂ hard core-soft shell abrasive and its CMP behavior on sapphire substrate, *J. Electron. Mater.* 49 (2020) 1301–1307, <https://doi.org/10.1007/s11664-019-07683-9>.